

Short Communication

# Microporous ZSM-5 zeolite anchors the exceptionally active triplet oxygen species: Mechanistic studies

Gang Yang<sup>a,b,\*</sup>, Jing Guan<sup>a</sup>, Lijun Zhou<sup>b</sup>, Xianchun Liu<sup>a</sup>, Xiuwen Han<sup>a</sup>, Xinhe Bao<sup>a</sup>

<sup>a</sup> State Key Laboratory of Catalysis, Dalian Institute of Chemical Physics, Chinese Academy of Sciences, 457 Zhongshan Road, Dalian 116023, PR China

<sup>b</sup> Key Laboratory of Forest Plant Ecology, Northeast Forestry University, Ministry of Education, Harbin 150040, PR China

Received 26 April 2007; received in revised form 3 December 2007; accepted 4 December 2007

Available online 14 December 2007

## Abstract

Through density functional calculations, it was found that the Brønsted acidic sites in microporous zeolites (e.g., ZSM-5) can stabilize and anchor the active triplet oxygen species [i.e.,  $O(^3P)$ ], thus providing an ideal locale for the related catalytic processes. An exemplified catalytic cycle was proposed here. The 419.3 nm photolysis of singlet  $N_2O$  leads to the formation of triplet  $N_2O$ , which releases the  $O(^3P)$  species almost without energy barrier. The  $O(^3P)$  species produced this way efficiently oxidizes CO into triplet  $CO_2$ , with the activation barrier computed to be  $0.13 \text{ kcal mol}^{-1}$  (zero point energy corrected).

© 2007 Elsevier Inc. All rights reserved.

**Keywords:** Catalysis; Density functional; Selective oxidation; Triplet oxygen species; Zeolite

## 1. Introduction

Up to date, the selective oxidations of aliphatic and aromatic hydrocarbons still represent one of the most challenged topics to us all [1]. Varieties of catalytic systems have been exploited [1–14], including the Cu or Fe-exchanged H-ZSM-5 zeolite with  $N_2O$  as the oxidant [4–14]. For the Fe/H-ZSM-5 catalysts, most researchers [4–12] have arrived to the agreement that the presence of some extra-framework Fe ions is indispensable to the formation of active “ $\alpha$ -oxygen” species. The “ $\alpha$ -oxygen” species was generated by the decomposition of  $N_2O$  on the Fe sites, which then reacted with the incoming hydrocarbons and completed the oxidation cycle. Kubánek et al. [5] and Kiwi-Minsker et al. [6] found that the catalytic perfor-

mances are quantitatively correlated with the contents of the Fe sites in Fe/H-ZSM-5 zeolite. On the contrary, Burch and Howitt [13] and Pietrzyk et al. [14] insisted that in the absence of the Fe species, the selective oxidation reaction can also take place due to the catalytic roles played by the Brønsted acidic sites.

Using quantum Monte-Carlo and density functional theory, Grossman et al. [15] revealed that the triplet oxygen species of  $O(^3P)$  is an effective oxidant for the conversion of cyclopentadiene into 2-cyclopentenone or 3-cyclopentenone. Using vacuum-ultraviolet laser-induced fluorescence (VUV-LIF) technique, it was found that the  $O(^3P)$  species can be obtained through the photolysis of singlet  $N_2O$  [16]. As indicated by Chang and Yarknoy [17] and Monfort et al. [18], the direct dissociation of the singlet  $N_2O$  to form the  $O(^3P)$  species is spin-forbidden. Enlightened by the above results, a catalytic oxidation system with the singlet  $N_2O$  and H-ZSM-5 zeolite as the starting materials was designed in the present communication, see the catalytic processes sketched in Fig. 1: (1) The singlet  $N_2O$  molecule was adsorbed on H-ZSM-5 zeolite and then excited to the triplet state, i.e., in the form of  $N_2O(^3\Pi)$ . (2) The triplet

\* Corresponding author. Address: State Key Laboratory of Catalysis, Dalian Institute of Chemical Physics, Chinese Academy of Sciences, Hexing Road 26, 457 Zhongshan Road, Dalian 116023, PR China. Tel.: +86 411 84379528; fax: +86 411 84694447.

E-mail addresses: [dicpyanggang@yahoo.com.cn](mailto:dicpyanggang@yahoo.com.cn) (G. Yang), [xhbaod@dicp.ac.cn](mailto:xhbaod@dicp.ac.cn) (X. Bao).

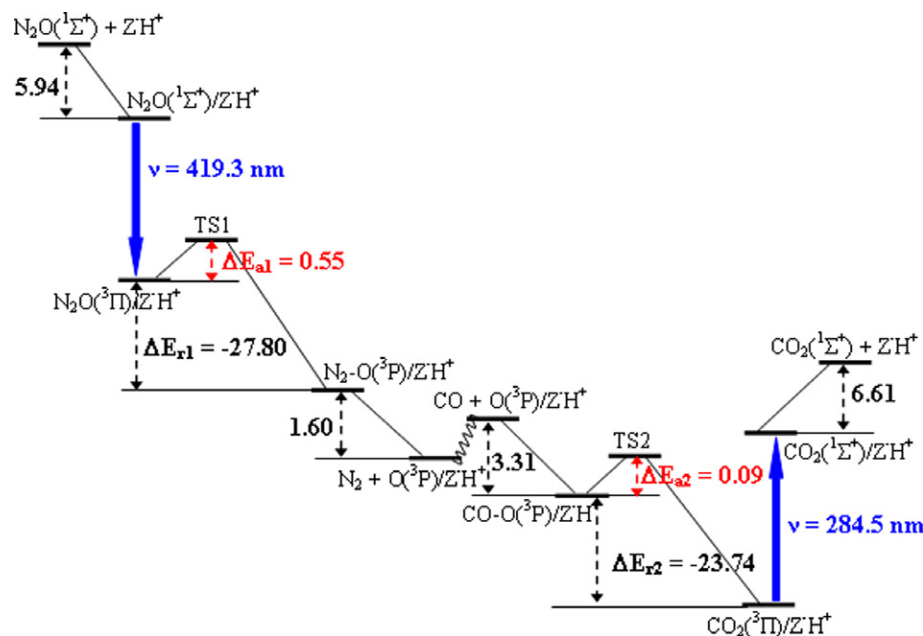


Fig. 1. The energy profile for reactions related with  $O(^3P)$  species anchored by H-ZSM-5 zeolite.

$N_2O(^3\Pi)$  was decomposed and released the active  $O(^3P)$  species, which was anchored tightly by H-ZSM-5 zeolite. (3) To test the catalytic reactivity of the  $O(^3P)$  species, the oxidation of carbon monoxide was chosen as the model reaction, which will produce the triplet  $CO_2$ . (4) The  $CO_2$  molecule in triplet state was converted into singlet state, thus completing the whole catalytic cycle. Note that it is also a way to convert the harmful  $N_2O$  into the useful intermediate of the triplet oxygen species.

## 2. Computational details

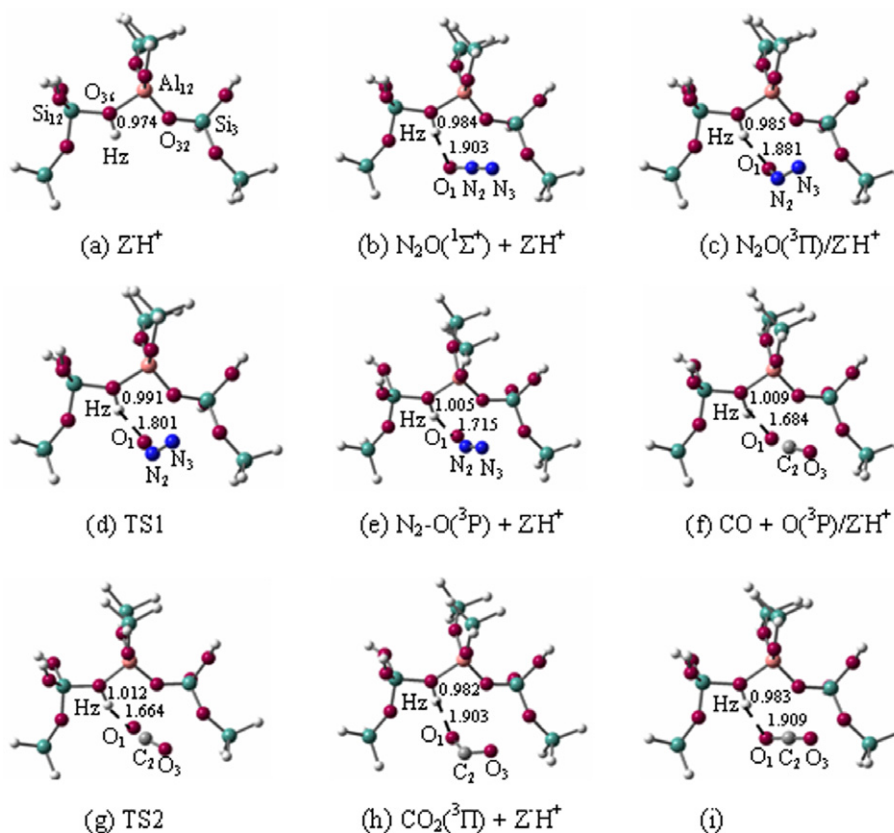
First principles density functional calculations were performed using the B3LYP/6-31G(d) methods [19,20] implemented in Gaussian98 program [21]. In zeolite calculations, the B3LYP method can obtain comparable results with MP2 method and provide good description of reaction profiles [22]. Accordingly, the B3LYP functional was widely used in the previous zeolite calculations [7–9,11,23,24]. To confirm the validity of 6-31G(d) basis set in dealing with the triplet species, two larger basis sets of 6-311G(d, p) and 6-311++G(d, p) were also employed to study the  $N_2O(^3\Pi)$  dissociation reactions in bare models. Noting that in the present work, the cluster models with and without the inclusion of H-ZSM-5 zeolite frameworks were designated as zeolite and bare models, respectively. All the transition states were determined utilizing the Synchronous Transit Quasi Newton (STQN) technique, followed by frequency calculations ensuring that only one imaginary vibration corresponds to the transition state. The zero point energy (ZPE) corrections were made in the calculations of activation barriers and reaction heats.

The structures of H-ZSM-5 zeolite were represented with clusters containing seven T sites (Fig. 2), with the Al

atom occupying one of the T12 sites. Our zeolite models are larger than the usually adopted five T ones [9,23,24]. To retain the local structures of H-ZSM-5 zeolite, the boundary Si and O atoms were fixed in their crystallographic positions as reported by Olson et al. [25] and Hodgson et al. [26].

## 3. Results and discussion

To better understand the role of H-ZSM-5 zeolite, the reactions described in Fig. 1 were first studied with bare models, see Fig. S1. In  $N_2O(^1\Sigma^+)$ , the  $O_1-N_2$  and  $N_2-N_3$  distances and  $O_1-N_2-N_3$  angle were optimized at 1.194 and 1.135 Å and 179.94°, respectively (Table 1 and Fig. S2). The wavelength for the excitation of  $N_2O(^1\Sigma^+)$  to the triplet state was calculated to be 424.0 nm, which is of the same order with the experimental value of 193 nm [16]. Compared with  $N_2O(^1\Sigma^+)$ ,  $N_2O(^3\Pi)$  has larger  $O_1-N_2$  and  $N_2-N_3$  distances of 1.281 and 1.216 Å and a smaller  $O_1-N_2-N_3$  angle of 121.79°. The triplet  $N_2O$  is ready to decompose into  $N_2$  and  $O(^3P)$  fragments, since the activation barrier was calculated at 2.58 kcal mol<sup>-1</sup> after ZPE corrections. The transition state has the negative frequency of -673.8 cm<sup>-1</sup>. The  $O_1-N_2$  distances in the transition state and product were equilibrated at 1.506 and 3.001 Å, respectively. The  $N_2-N_3$  bond in the product is typical of triple bond (Table 1). The reaction heat of  $N_2O(^3\Pi)$  dissociation amounts to -21.38 kcal mol<sup>-1</sup> after ZPE corrections (Table S1). As shown in Table S2, the larger basis sets exert unobvious effects on the geometries; however, some changes were observed in the activation barriers, which equal 2.97 and 2.78 kcal mol<sup>-1</sup> with 6-311G(d, p) and 6-311++G(d, p) basis sets, respectively. The effect of basis sets on the activation barrier is not so distinct as that of zero point

Fig. 2. Cluster models representing reactions of  $\text{N}_2\text{O}$  decomposition and CO oxidation in H-ZSM-5 zeolite.Table 1  
Geometries and stabilization energies for reactions related with  $\text{O}(^3\text{P})$  species

	$\text{O}_1\text{-N}_2$ ( $\text{O}_1\text{-C}_2$ )/Å		$\text{N}_2\text{-N}_3$ ( $\text{C}_2\text{-O}_3$ )/Å		$\text{O}_1\text{-N}_2\text{-N}_3$ ( $\text{O}_1\text{-C}_2\text{-O}_3$ )/°		$\Delta E_{\text{sta}}/\text{kcal mol}^{-1}$
	Bare	Zeolite	Bare	Zeolite	Bare	Zeolite	
$\text{N}_2\text{O}(^1\Sigma^+)$	1.194	1.202	1.135	1.128	179.94	178.40	-5.94
$\text{N}_2\text{O}(^3\Pi)$	1.281	1.322	1.216	1.202	121.79	120.88	-5.17
TS1	1.506	1.443	1.157	1.171	118.70	119.12	-8.30
$\text{N}_2/\text{O}(^3\text{P})$	3.001	3.130	1.106	1.105	162.56	141.35	-12.52
$\text{O}(^3\text{P})$							-11.29
$\text{CO}/\text{O}(^3\text{P})$	2.585	2.407	1.137	1.136	141.98	141.26	-13.49
TS2	2.178	2.142	1.138	1.367	123.53	131.98	-13.57
$\text{CO}_2(^3\Pi)$	1.261	1.251	1.237	1.248	118.44	119.53	-4.80
$\text{CO}_2(^1\Sigma^+)$	1.169	1.176	1.169	1.162	179.80	176.98	-6.61

energies (ZPE), and therefore the 6-31G(d) basis was used exclusively in the following discussions. The separation of  $\text{O}(^3\text{P})$  and  $\text{N}_2$  fragments in the product is endothermic and needs energy of  $0.38 \text{ kcal mol}^{-1}$ . Afterwards, the incoming CO molecule attacks the  $\text{O}(^3\text{P})$  species, with the  $\text{O}_1\text{-C}_2$  and  $\text{C}_2\text{-O}_3$  distances in the initial structure optimized at 2.585 and 1.137 Å, respectively. This oxidation reaction produces triplet  $\text{CO}_2$ , where two C–O distances and OCO angle were calculated at 1.237, 1.261 Å and  $118.44^\circ$ , respectively. The transition state has  $\text{O}_1\text{-C}_2$  distance of 2.178 Å with the only imaginary vibration of  $-112.6 \text{ cm}^{-1}$ . The activation barrier was calculated to be  $0.18 \text{ kcal mol}^{-1}$  after ZPE corrections.  $\text{CO}_2(^3\Pi)$  will be converted into the singlet state and meanwhile release the light

with a theoretical wavelength of 289.7 nm. It is worth noting that at the singlet state,  $\text{N}_2\text{O}$  and  $\text{CO}_2$  are linear molecules whereas they are both severely curved at the triplet state (Table 1).

In H-ZSM-5 zeolite cluster (Fig. 2a), the  $\text{O}_{36}\text{-Hz}$  distance was equilibrated at 0.974 Å, consistent with the B3LYP/6-31G(d, p) values of ca. 0.970 Å [27]. Upon  $\text{N}_2\text{O}(^1\Sigma^+)$  adsorption (Fig. 2b), the  $\text{O}_1\text{-N}_2$  and  $\text{O}_{36}\text{-Hz}$  bonds were slightly elongated whereas the  $\text{N}_2\text{-N}_3$  bond slightly shortened. Hydrogen bond was formed between Hz and  $\text{O}_1$  atoms with the distance of 1.903 Å. The  $\text{N}_2\text{O}(^1\Sigma^+)$  adsorption process is thermodynamically favoured by energy of  $-5.94 \text{ kcal mol}^{-1}$ . With the exposure to the light with a theoretical wavelength of 419.3 nm, the adsorbed  $\text{N}_2\text{O}(^1\Sigma^+)$

will be converted to the triplet state (Fig. 2c), where stronger hydrogen bonding is formed as evidenced by the shorter O<sub>1</sub>–Hz distance of 1.881 Å. The O<sub>1</sub>–N<sub>1</sub> distance in adsorbed N<sub>2</sub>O(<sup>3</sup>Π) equals 1.322 Å and is larger than that in bare models. As a result, the activation barrier becomes smaller and equals 0.55 kcal mol<sup>-1</sup>, 15.0% of that in bare models. After ZPE corrections, the activation barrier is equal to -0.19 kcal mol<sup>-1</sup>, implying that the N<sub>2</sub>O(<sup>3</sup>Π) dissociation takes place automatically [16,28]. The N<sub>2</sub>O(<sup>3</sup>Π) dissociation reaction has an early transition state (Fig. 2d) with the O<sub>1</sub>–N<sub>1</sub> distance of 1.443 Å shorter than the value of 1.506 Å in bare models. As to the product of N<sub>2</sub>O(<sup>3</sup>Π) dissociation reaction (Fig. 2e), the O(<sup>3</sup>P) and N<sub>2</sub> fragments were parted with the O<sub>1</sub>–N<sub>2</sub> distance of 3.130 Å. Besides the negative vibration of -517.7 cm<sup>-1</sup>, the transition state of the N<sub>2</sub>O(<sup>3</sup>Π) dissociation reaction was substantiated by the results of intrinsic reaction coordinate (IRC) computations (Fig. 3). The IRC results were obtained by fixing the O<sub>1</sub>–N<sub>2</sub> distance at different values, and all the other geometric parameters such as the O<sub>1</sub>N<sub>2</sub>N<sub>3</sub> angle were freely optimized and will change synchronously with the elongation of the O<sub>1</sub>–N<sub>2</sub> distance. Contrary to the endothermic process in bare models, the desorption of N<sub>2</sub> from O(<sup>3</sup>P)/H-ZSM-5 zeolite is exothermic (-1.60 kcal mol<sup>-1</sup>). H-ZSM-5 zeolite well stabilizes the active O(<sup>3</sup>P) species through the strong hydrogen bonding (Hz–O<sub>1</sub>: 1.715 Å).

The structure of CO adsorption on O(<sup>3</sup>P)/H-ZSM-5 zeolite was shown in Fig. 2f. The O<sub>1</sub>–C<sub>2</sub> distance was calculated to be 2.407 Å and is shorter than the value in bare models (Table 1). The adsorption energy of CO was obtained at -3.31 kcal mol<sup>-1</sup>. As a result of the shortened O<sub>1</sub>–C<sub>2</sub> distance compared with bare models, the activation barrier is less than that in bare models and equals 0.13 kcal mol<sup>-1</sup> after the inclusion of ZPE corrections. Similar to the N<sub>2</sub>O(<sup>3</sup>Π) dissociation process, the CO oxidation (Fig. 2g) also has an early transition state with the O<sub>1</sub>–C<sub>1</sub> distance of 2.142 Å. The characteristic frequency of the transition state was situated at -75.0 cm<sup>-1</sup>. The transition

state is highly stabilized by the forceful hydrogen bonding with the acidic Hz site (Hz–O<sub>1</sub>: 1.664 Å), at the expense of the elongation of O<sub>36</sub>–Hz distance. In the product (Fig. 2h), the interaction with H-ZSM-5 zeolite becomes weakened, with the Hz–O<sub>1</sub> distance optimized at 1.903 Å. The difference between the two C–O distances of CO<sub>2</sub>(<sup>3</sup>Π) was neglectable (0.003 Å), whereas in bare models it amounts to 0.024 Å (Table 1). The wavelength for the conversion from triplet state to singlet state (Fig. 2i) was calculated to be 284.5 nm. The adsorbed singlet CO<sub>2</sub> is almost linear with the C–O bond towards the acidic Hz site elongated by 0.014 Å than the other. The Hz–O<sub>1</sub> hydrogen bond was equilibrated at 1.909 Å which is slightly longer than that in triplet state. The catalytic cycle was completed with CO<sub>2</sub>(<sup>1</sup>Σ<sup>+</sup>) desorbed from H-ZSM-5 zeolite, requiring an energy of 6.61 kcal mol<sup>-1</sup>. In this way, H-ZSM-5 zeolite is restored to the original state and prepared for the next catalytic cycle, see Fig. 1.

As aforementioned, H-ZSM-5 zeolite exerts remarkable influences on the catalytic processes, e.g., lowering the activation barriers of N<sub>2</sub>O(<sup>3</sup>Π) decomposition and CO oxidation reactions and turning the endothermic N<sub>2</sub> and O(<sup>3</sup>P) separation process into exothermic. The related geometric parameters were also greatly affected, and the details can be found in Table 1. However, we consider that the most important role of H-ZSM-5 zeolite is to provide an ideal locale for the catalytic processes to take place. The reactants, intermediates, products as well as transition states are highly stabilized by the presence of H-ZSM-5 zeolite, which can be estimated with the equation below:

$$E_{\text{sta}} = E(X/\text{H-ZSM-5}) - E(\text{H-ZSM-5}) - E(X) \quad (1)$$

where  $E(X/\text{H-ZSM-5})$  represents the energy of zeolite models adsorbed with  $X$  species, whereas  $E(X)$  and  $E(\text{H-ZSM-5})$  denote the energies of  $X$  species in bare models and H-ZSM-5 zeolite, respectively.

The stabilization energies ( $E_{\text{sta}}$ ) of all the investigated species were calculated and listed in Table 1. The uniformly negative values indicate that all the species are stabilized by H-ZSM-5 zeolite. It is well-known that the triplet  $O$  species is quite active; however, it is highly stabilized by H-ZSM-5 zeolite with the large stabilization energy of -11.29 kcal mol<sup>-1</sup>. Among all the species, the transition states are usually considered as the most unstable. Owing to the presence of H-ZSM-5 zeolite, the two transition states are well stabilized with the stabilization energies calculated at -8.30 and -13.57 kcal mol<sup>-1</sup>, respectively. The large stabilization energies ensure the preferential adsorption on the Brønsted acidic sites, which is differentiated essentially from the irregular collisions in the absence of H-ZSM-5 zeolite.

On Fe/H-ZSM-5 zeolite, the release of active “α-oxygen” species by N<sub>2</sub>O(<sup>1</sup>Σ<sup>+</sup>) decomposition necessitates energy barriers beyond 30.0 kcal mol<sup>-1</sup> [8,29]. The direct decomposition of N<sub>2</sub>O(<sup>1</sup>Σ<sup>+</sup>) was also considered, both in bare and zeolite models, and the results show that it is an implausible way to obtain active oxygen species [17,18]. As Fig. 1 shows, each elementary step requires energy well

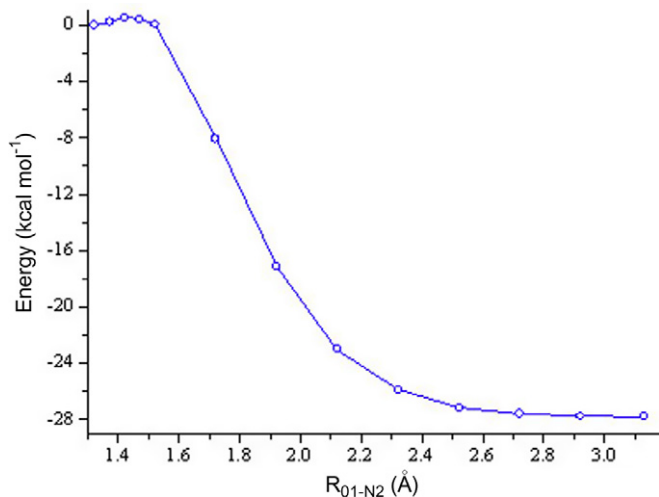


Fig. 3. Intrinsic reaction coordinate of N<sub>2</sub>O(<sup>3</sup>Π) dissociation in H-ZSM-5 zeolite.

below 30.0 kcal mol<sup>-1</sup>. Accordingly, the catalytic cycle proposed here is practical, where the active O(<sup>3</sup>P) species, generated by N<sub>2</sub>O(<sup>1</sup>Σ<sup>+</sup>) excitation followed by decomposition, is an efficient oxidant such as the presently studied CO oxidation reaction.

#### 4. Concluding remarks

In this work, a catalytic cycle was proposed with the aid of density functional calculations. At the Brønsted acidic sites of nanostructural ZSM-5 zeolite, the singlet N<sub>2</sub>O was photolyzed with the wavelength of 419.3 nm to form the triplet N<sub>2</sub>O, which is ready to decompose into the N<sub>2</sub> and O(<sup>3</sup>P) species. The active O(<sup>3</sup>P) species is an efficient oxidant and can catalyze many types of reactions such as the presently studied CO oxidation to form CO<sub>2</sub>. The results showed that the Brønsted acidic sites in ZSM-5 zeolite can effectively stabilize and anchor the active O(<sup>3</sup>P) species as well as other related species. Accordingly, the nanostructural zeolites provide an ideal locale for the related catalytic processes to take place.

#### Appendix A. Supplementary information available

Supplementary data associated with this article can be found, in the online version, at [doi:10.1016/j.micromeso.2007.12.002](https://doi.org/10.1016/j.micromeso.2007.12.002).

#### References

- [1] C.G. Jia, T. Kitamura, Y. Fujiwara, *Acc. Chem. Res.* 34 (2001) 633.
- [2] A.A. Fokin, P.R. Schreiner, *Chem. Rev.* 101 (2002) 1551.
- [3] T.V. Choudhary, E. Aksoylu, D.W. Goodman, *Catal. Rev.* 45 (2003) 151.
- [4] G.I. Panov, V.I. Sobolev, A.S. Kharitonov, *J. Mol. Catal.* 61 (1990) 85.
- [5] P. Kubánek, B. Wichterlová, Z. Sobalík, *J. Catal.* 211 (2002) 109.
- [6] L. Kiwi-Minsker, D.A. Bulushev, A. Renken, *J. Catal.* 219 (2003) 273.
- [7] A.L. Yakovlev, G.M. Zhidomirov, R.A. van Santen, *J. Phys. Chem. B* 105 (2001) 12297.
- [8] J.A. Ryder, A.K. Chakraborty, A.T. Bell, *J. Phys. Chem. B* 106 (2002) 7059.
- [9] K. Yoshizawa, Y. Shiota, K. Takashi, *J. Phys. Chem. B* 107 (2003) 11404.
- [10] A. Zecchina, M. Rivallan, G. Berlier, C. Lamberti, G. Ricchiardi, *Phys. Chem. Chem. Phys.* 9 (2007) 3483.
- [11] P.M. Esteves, B. Louis, *J. Phys. Chem. B* 110 (2006) 16793.
- [12] Z.Q. Liu, P.J. Millington, J.E. Bailie, R.R. Rajaram, J.A. Anderson, *Microporous Mesoporous Mater.* 104 (2007) 159.
- [13] R. Burch, C. Howitt, *Appl. Catal. A* 103 (1993) 135.
- [14] P. Pietrzyk, B. Gil, Z. Sojka, *Catal. Today* 126 (2007) 103.
- [15] J.C. Grossman, W.A. Lester Jr., S.G. Louie, *J. Am. Chem. Soc.* 122 (2000) 705.
- [16] S. Nishida, K. Takahashi, Y. Matsumi, *J. Phys. Chem. A* 108 (2004) 2451.
- [17] A.H.H. Chang, D.R. Yarknony, *J. Chem. Phys.* 99 (1993) 6824.
- [18] X.S. Monfort, M. Sodupe, V. Branchadell, *Chem. Phys. Lett.* 368 (2003) 242.
- [19] A.D. Becke, *Phys. Rev. A* 38 (1988) 3098.
- [20] C. Lee, W. Yang, R.G. Parr, *Phys. Rev. B* 37 (1988) 785.
- [21] M.J. Frisch, G.W. Trucks, H.B. Schlegel, G.E. Scuseria, M.A. Robb, J.R. Cheeseman, V.G. Zakrzewski, J.A. Montgomery Jr., R.E. Stratmann, J.C. Burant, S. Dapprich, J.M. Millam, A.D. Daniels, K.N. Kudin, M.C. Strain, O. Farkas, J. Tomasi, V. Barone, M. Cossi, R. Cammi, B. Mennucci, C. Pomelli, C. Adamo, S. Clifford, J. Ochterski, G.A. Petersson, P.Y. Ayala, Q. Cui, K. Morokuma, D.K. Malick, A.D. Rabuck, K. Raghavachari, J.B. Foresman, J. Cioslowski, J.V. Ortiz, A.G. Baboul, B.B. Stefanov, G. Liu, A. Liashenko, P. Piskorz, I. Komaromi, R. Gomperts, R.L. Martin, D.J. Fox, T. Keith, M.A. Al-Laham, C.Y. Peng, A. Nanayakkara, C. Gonzalez, M. Challacombe, P.M.W. Gill, B. Johnson, W. Chen, M.W. Wong, J.L. Andres, C. Gonzalez, M. Head-Gordon, E.S. Replogle, J.A. Pople, *Gaussian 98*, Revision A.9 Gaussian, Inc., Pittsburgh, PA, 1998.
- [22] S.A. Zygmunt, R.M. Mueller, L.A. Curtiss, L.E. Iton, *J. Mol. Struct. (Theochem.)* 430 (1998) 9.
- [23] G. Yang, L.J. Zhou, X.C. Liu, X.W. Han, X.H. Bao, *J. Phys. Chem. B* 110 (2006) 22295.
- [24] G. Yang, L.J. Zhou, X.C. Liu, X.W. Han, X.H. Bao, *Catal. Commun.* 8 (2007) 1981.
- [25] D.H. Olson, G.T. Kokotallo, S.L. Lawton, W.M. Meier, *J. Phys. Chem.* 85 (1981) 2238.
- [26] A.E.A. Swaisgood, M.K. Barr, P.J. Hay, A. Redondo, *J. Phys. Chem.* 95 (1991) 10031.
- [27] G. Yang, X.C. Liu, X.W. Han, X.H. Bao, *J. Phys. Chem. B* 110 (2006) 23388.
- [28] D.Y. Hwang, A.M. Mebel, *Chem. Phys.* 259 (2000) 89.
- [29] A. Martínez, A. Goursot, B. Coq, G. Belahay, *J. Phys. Chem. B* 108 (2004) 8823.